CHEMISTRY
A European Journal

www.chemeurj.org

Reprint

A Journal of
ChemPubSoc Europe
ACES
Asian Chemical Editorial Society
WILEY-VCH

ChemPubSoc Europe

DOI: 10.1002/chem.201902183

CHEMISTRY
A European Journal
Full Paper

DNA Structures

Targeting G-Rich DNA Structures with Photoreactive Bis-Cyclometallated Iridium(III) Complexes

Justin Weynand,[a, b] Hughes Bonnet,[b] Frédérique Loiseau,[b] Jean-Luc Ravanat,[c] Jérôme Dejeu,[b] Eric Defrancq,*[b] and Benjamin Elias*[a]

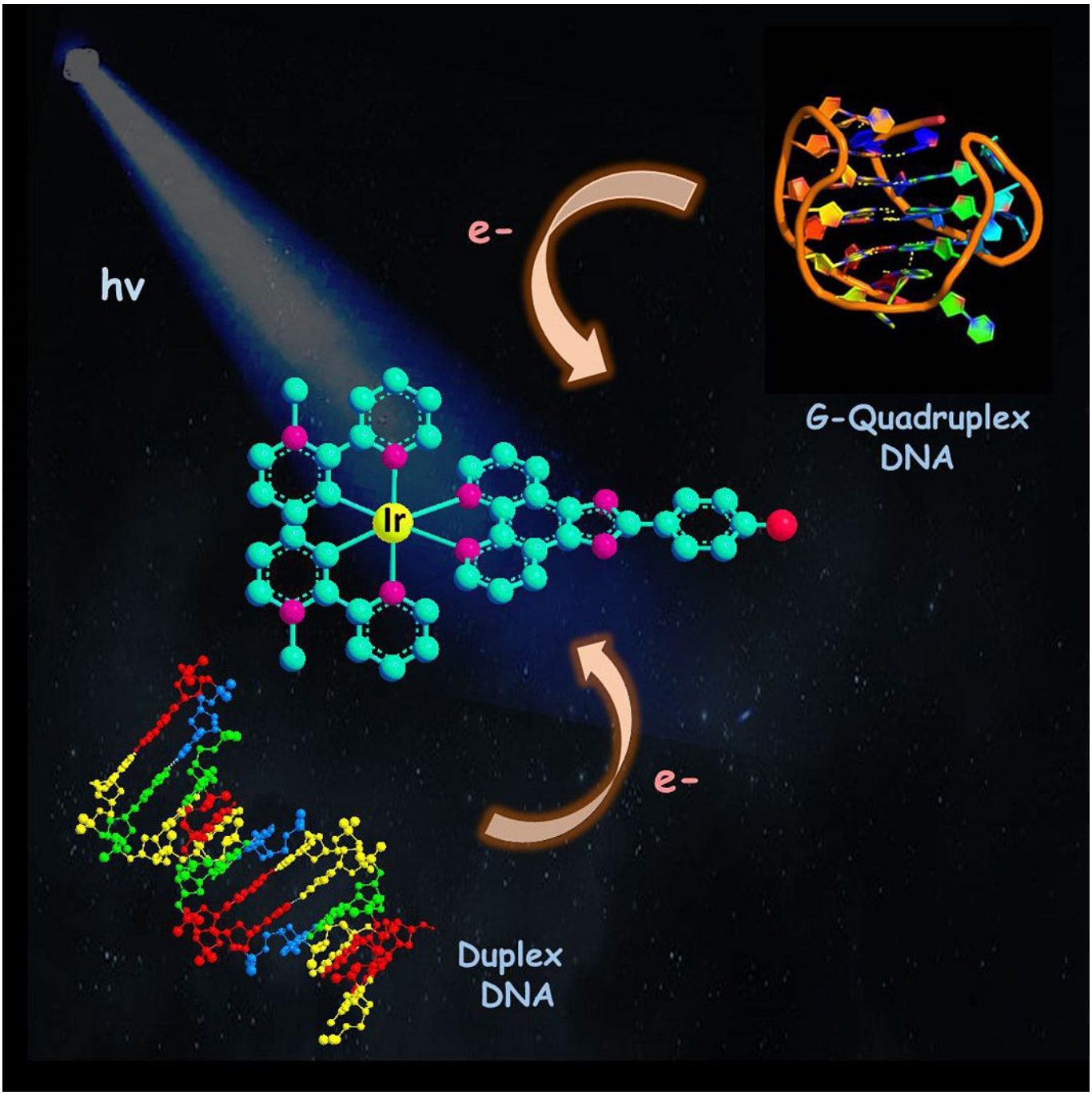

Abstract: The synthesis and characterisation of three novel iridium(III) bis-cyclometallated complexes is reported. Their photophysics have been fully characterised by classical methods and revealed charge-transfer (CT) and ligand-centred (LC) transitions. Their ability to selectively interact with G-quadruplex telomeric DNA over duplex DNA has been studied by circular dichroism (CD), bio-layer interferometry (BLI) and surface plasmon resonance (SPR) analyses. Interestingly, one of the complexes was able to promote photoinduced electron transfer (PET) with the guanine DNA base, which in turn led to oxidative damage (such as the formation of 8-oxoguanine) to the telomeric sequence. To the best of our knowledge, this is the first study of highly photo-oxidising bis-cyclometallated iridium(III) complexes with G-quadruplex telomeric DNA.

Introduction

The double-helical structure of DNA, in which two anti-parallel strands are held together through canonical A/T and G/C base pairing, was resolved over half a century ago. Beyond canonical double-helical-based structures such as B-DNA, A-DNA and Z-DNA, the past decades have brought accumulating evidence of the existence and biological relevance of four-stranded nucleic acid motifs. In particular, guanine-rich nucleic acids can adopt peculiar secondary structures, globally known as G-quadruplex nucleic acid (G4-DNA and G4-RNA).[1] They consist of stacked tetrads of Hoogsteen hydrogen-bonded guanine bases connected by various loop-forming sequences and are stabilised by physiologically abundant K^+ and Na^+ cations. Sequencing and bioinformatics analyses of the human genome indicate that it contains as many as 700 000 sequences having the potential to form stable G-quadruplex structures.[2,3] G4-DNA-forming sequences are found in the promoter regions of a large number of genes, including the proto-oncogenes c-MYC, c-KIT, and KRAS, as well as in the viral genome.[4,5] The most-documented biological function of G-quadruplexes concerns telomere homeostasis.[6] Telomeric DNA are guanine-rich sequences found in the extremity of the genome. They have critical roles in the life of cells, such as protecting the chromosome or being involved in the senescence process.[7–9] The telomeres of healthy cells progressively decrease after each cell division until reaching a critical length (Hayflick limit) at which the cells divide no further and enter into senescence. However, in cancer cells, the Hayflick limit is never reached, thus preventing senescence and leading to cell immortality. Two main processes are involved in telomere maintenance: 1) telomerase overexpression, which can elongate the telomeric sequence [10] or 2) the alternative lengthening of telomeres (ALT) based on a homologous recombination mechanism.[11]

The stabilisation of G-quadruplexes by small organic molecules[12] or metal complexes[13] has been the subject of much intense research over the past decade with the aim to design molecules displaying a good affinity for G4-DNA and selectivity for G-quadruplex over duplex DNA. This approach is now considered a useful molecular tool to enhance and/or promote quadruplex-related biological effects in cells and shows high potential for future therapies.[14]

In this context, metal complexes show a number of advantages in comparison with organic compounds. They have a net positive charge, a tuneable geometry and many of them show exploitable photochemical properties. Therefore, many metal complexes have been designed to stabilise G-quadruplex DNA to prevent the telomerase action. These metal complexes include nickel(II) salphen[15] and platinum(II)[16] and ruthenium(II) polypyridine complexes.[17] Very few metal complexes able to target and cause photodamage to G-quadruplex DNA have been reported.[18] Recently, Thomas and co-workers reported the use of a dinuclear ruthenium(II) complex able to photo-oxidise guanosine moieties in duplex and G-quadruplex DNA.[18a] We also reported on new tetraazaphenanthrene (TAP) ruthenium(II) complexes that can selectively interact with G-quadruplex over duplex DNA and are able to trigger photoinduced electron transfer (PET) with the guanine base.[18b] Interestingly, these complexes described by Thomas and co-workers and by us showed very interesting photocytotoxic effects.

Cyclometallated iridium(III) complexes have also been extensively studied owing to their photophysical and -chemical properties, including high luminescence quantum yields, long excited-state lifetimes, large Stoke's shifts and strong photostability. Various applications, including in organic light-emitting diodes (OLEDs)[19] or photocatalytic hydrogen production,[20] have been reported. However, in the context of G-quadruplex DNA, few cyclometallated iridium complexes have been described. Ma and co-workers have explored a variety of mononuclear iridium(III) complexes as G-quadruplex-selective probes for the construction of a range of label-free luminescent detection platforms.[21] Additionally, Sleiman and co-workers reported the complex $[Ir(ppy)_2(CPIP)]^+$ (**1**) based on 2-phenylpyridine (ppy) and 2-(4-chlorophenyl)-1*H*-imidazo[4,5-*f*][1,10]phenanthroline (CPIP), luminescence studies of which revealed its high

[a] *J. Weynand, B. Elias*
Institut de la Matière Condensée et des Nanosciences (IMCN)
Molecular Chemistry, Materials and Catalysis (MOST)
Université catholique de Louvain (UCLouvain)
Place Louis Pasteur 1, bte L4.01.02, 1348 Louvain-la-Neuve (Belgium)
E-mail: Benjamin.Elias@uclouvain.be

[b] *J. Weynand, H. Bonnet, F. Loiseau, J. Dejeu, E. Defrancq*
CNRS, DCM UMR5250, Université Grenoble Alpes
38000 Grenoble (France)
E-mail: Eric.Defrancq@univ-grenoble-alpes.fr

[c] *J.-L. Ravanat*
CEA, CNRS, INAC-SyMMES, Université Grenoble Alpes
17 rue des martyrs, 38054, Grenoble CEDEX 9 (France)

Supporting information and the ORCID identification number(s) for the author(s) of this article can be found under: https://doi.org/10.1002/chem.201902183.

ability to selectively probe G-quadruplex DNA over duplex DNA.[22] We have recently reported a study of bis-cyclometallated and bis-tridentate iridium complexes with the ability to promote photoinduced electron transfer (PET) with guanine and adenine DNA bases as a result of π-deficient ancillary ligands.[23]

In this context, we envisaged developing new bis-cyclometallated iridium(III) complexes that can interact and photoreact through type I and II photo-oxidation with genetic materials, in particular with telomeric G-quadruplex DNA. We report herein on the synthesis and characterisation of three new bis-cyclometallated iridium complexes (**2**–**4**) obtained by the coordination of two bis-cyclometallated ligands (2-phenylpyridine (ppy) or 1-methyl-[2,2′-bipyridin]-1-ium (2,2′-C^N)) and a diimine ligand (CPIP or 2-(4-chlorophenyl)-1*H*-imidazo[4,5-*f*]pyrazino[2,3-*h*]quinoxaline (CPITAP)). The CPIP ligand was chosen because it has been reported as an efficient G-quadruplex ligand (see above)[18b,22] and CPITAP is based on the CPIP ligand, the phenanthroline moiety being replaced by the more π-deficient TAP group. Complexes based on (2,2′-C^N) ancillary ligands have the advantage of being highly soluble in aqueous solvent as a result of their positive charges.[24] The photophysical properties of compounds **1**–**4** were investigated and the results indicated mixed charge-transfer (CT) and ligand-centred (LC) transitions. Interestingly, as evidenced by luminescence spectroscopy, complexes **3** and **4** are highly oxidising under light irradiation. The affinity and selectivity of complexes **3** and **4** towards G-quadruplex DNA were studied by CD melting (T_m), bio-layer interferometry (BLI) and surface plasmon resonance (SPR) analyses.

Results and Discussion

Synthesis of complexes 1–4

The CPIP and CPITAP ligands were prepared according to methodologies previously described in the literature. Briefly, the CPIP ligand was synthesised by the condensation of 4-chlorobenzaldehyde with 1,10-phenanthroline-5,6-dione in an ammonium medium (Scheme 1).[22] The CPITAP ligand was obtained through the reaction of 4-chlorobenzaldehyde and 9,10-diamino-1,4,5,8-tetraazaphenanthrene in an acetic acid/ethanol mixture at reflux.[18b] The corresponding Ir^{III} complexes **1**–**4** were prepared by the direct chelation of the N^N ligand (CPIP or CPITAP) with an Ir^{III} precursor bearing either 2-phenylpyridine ($[Ir(ppy)_2Cl]_2$) or *N*-methylphenylpyridine ($[Ir(2,2'\text{-}C\text{^}N)_2Cl]_2$) ligands. Complexes **1**–**4** were purified by preparative SiO_2 chromatography to afford the pure hexafluorophosphate salts as the final compounds. The complexes were unambiguously characterised by ^1H NMR spectroscopy and HRMS (see the Experimental Section and Figures S1–S6 and S7–S9 in the Supporting Information) as well as by UV/Vis, cyclic voltammetry (CV) and photochemical studies (see below).

Absorption and luminescence properties

The photophysical properties of complexes **1**–**4** were assessed in acetonitrile and water. The absorption spectra of complexes

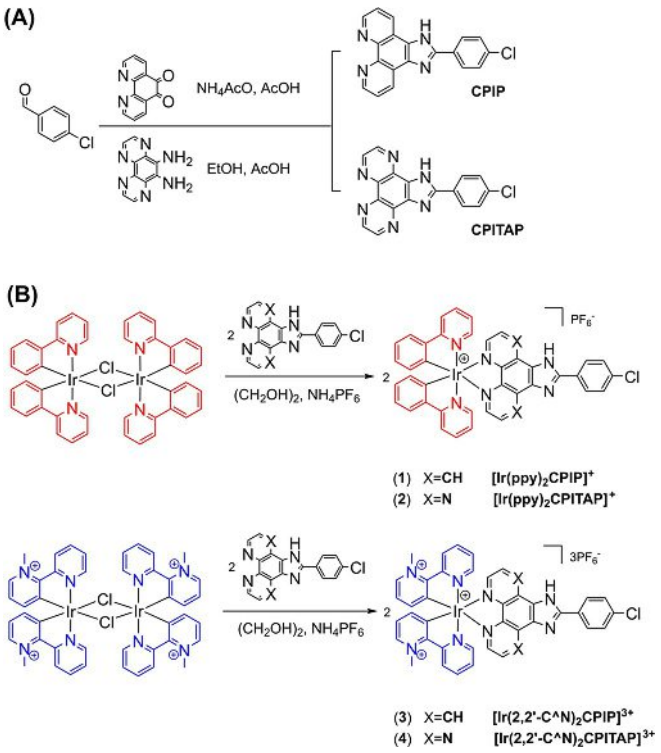

Scheme 1. Synthesis of (A) the CPIP and CPITAP ligands and (B) Ir^{III} complexes **1**–**4**.

1–**4** in acetonitrile at 298 K are shown in Figure 1 and in the Supporting Information (see Figures S10 and S11). The corresponding spectroscopic data are summarised in Table 1. All the complexes display intense absorption bands in the UV region (250–300 nm) with high molar extinction coefficients ($\varepsilon > 20\,000\ M^{-1}\,cm^{-1}$). By comparison with the literature and the absorption spectra of the free ligands in solution, these bands have been assigned to ligand-centred (LC) transitions. At lower energy ($\lambda > 340$ nm), charge-transfer (CT) transitions can also

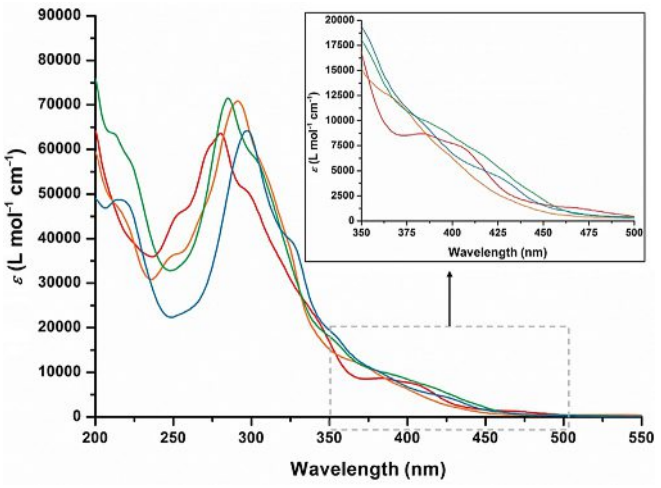

Figure 1. UV/Vis absorption spectra of complexes **1** (red), **2** (orange), **3** (green) and **4** (blue) in acetonitrile at 298 K. Inset: zoom of the 350–500 nm region.

Table 1. Absorption and luminescence data for complexes **1**–**4**.

Complex	λ_{Abs} [nm] (ε)[a]	λ_{Em} [nm][b]			Φ_{Em}[c]		τ [ns][d]	
	CH_3CN	CH_3CN	H_2O	77 K	CH_3CN	H_2O	CH_3CN	H_2O
1	453	583	n.d.	536	0.036	n.d.	67	n.d.
	(1.56)				(0.15)	n.d.	(441)	n.d.
2	400	697	n.d.	615	$<1\times10^{-3}$	n.d.	14	n.d.
	(6.27)				$<1\times10^{-3}$	n.d.	(12)	n.d.
3	417	528	528	504, 544	0.067	0.0018	613	316
	(6.40)				(0.136)	(0.0018)	(950)	(560)
4	429	528	528	504, 544	$<1\times10^{-3}$	$<1\times10^{-3}$	6	7
	(4.04)				(0.001)	$<1\times10^{-3}$	(9)	(8)

[a] λ of the most bathochromic absorption in MeCN (extinction coefficient, $\varepsilon\times10^3$ M^{-1} cm^{-1}). [b] λ at RT in MeCN, H_2O and at 77 K in EtOH/MeOH (4:1, v/v). n.d.: not determined due to the very low solubility of the chloride salt in water. [c] Quantum yield of emission measured by comparison with the reference $[Ru(bpy)_3]^{2+}$, determined in air and under argon (in parentheses). Excitation at 450 nm, errors are estimated to be 10%. [d] Luminescence lifetime (after irradiation at $\lambda=400$ nm) measured in air and under argon (in parentheses). Errors are estimated to be 5%.

be observed with lower molar extinction coefficients ($\varepsilon<20\,000$ M^{-1} cm^{-1}).

The emission spectra of complexes **1**–**4** were recorded in deoxygenated and oxygenated acetonitrile or water. The luminescence data are presented in Table 1 (see Figures S10–S13 in the Supporting Information).

Complex **1** exhibits luminescence in the orange region of the visible spectrum, consistent with the literature data.[22] The bathochromic shift of the emission of **2** compared with **1** can be explained by the stabilisation of the LUMO of the electron-deficient ligand CPITAP.

The emission spectra of complexes **1** and **2** in EtOH/MeOH (4:1, v/v) at 77 K are blueshifted compared with those recorded in organic solvent (Table 1), which provides some evidence for a charge-transfer (CT) character of the excited state. According to Coe and co-workers, the radiative process for Ir^{III} complexes bearing 2,2′-C^N ligands (such as **3** and **4**) can be ascribed to a mixture of ^{3}LC and ^{3}MLCT transitions.[25] It is therefore reasonable to assume that the same manifold of excited states is operative in our compounds, that is, complexes **3** and **4** should possess predominantly ^{3}LC (π(2,2′-C^N)→π^*(2,2′-C^N)) and ^{3}MLCT (dπ(Ir)→π^*(2,2′-C^N)) character.[25]

For all the complexes **1**–**4**, the quantum yields of emission (Φ) and luminescence lifetimes (τ) measured in acetonitrile increase on going from air to argon, which suggests their ability to photosensitise triplet oxygen into singlet oxygen. The low quantum yields for complex **4** in both organic and aqueous solvent and for complex **2** in organic solvent could be explained by an increase of the non-radiative process due to interactions of the solvent with the non-chelating nitrogen atoms of the CPITAP ligand. As complexes **1** and **2** are poorly soluble in aqueous solvent, no quantum yields or luminescence data could be obtained in water.

Electrochemical study

The redox properties of **1**–**4** were investigated by cyclic voltammetry experiments in dry deoxygenated acetonitrile; the data are presented in Table 2 (see also Figures S14–S17 in the Supporting Information).

Table 2. Electrochemical data for complexes **1**–**4**.[a]

Complex	$E_{1/2,ox}$ [V]	E^*_{ox} [V][b]	$E_{1/2,red}$ [V]	E^*_{red} [V][b]
1	+1.35	−0.78	−1.57	0.56
2	+1.38	−0.40	−0.72	1.06
3	>2	–[c]	−0.76	1.59
4	>2	–[c]	−0.76	1.59

[a] Data were measured at room temperature in deoxygenated MeCN with 0.1 M Bu_4NClO_4 as the supporting electrolyte (V vs. Ag/AgCl reference electrode). Complex concentration = 0.8 mM. [b] Excited-state potentials estimated from $E^*_{ox}=E_{1/2,ox}-E_{0\text{-}0}$ and $E^*_{red}=E_{1/2,red}+E_{0\text{-}0}$. The energy of the excited state, $E_{0\text{-}0}$, was assimilated to the maximum of the emission spectrum in acetonitrile at 298 K. [c] could not be estimated due to impossibility of measuring E_{ox} of the ground state.

Complexes **1** and **2** display a one-electron reversible oxidation wave, usually attributed to the oxidation of the Ir–phenylpyridine moiety.[22] For complexes **3** and **4**, no oxidation could be detected below 2 V versus Ag/AgCl, likely due to the presence of the pyridinium unit in the cyclometallated ligands stabilising the HOMO orbital of the complex. This is consistent with the oxidation data of similar complexes already published.[25] Indeed, Coe and co-workers described one irreversible oxidation for similar compounds in the region 2.2–2.5 V, which was assigned to the Ir^{IV}/Ir^{III} couple. For the reduction, the wave observed for complex **1** corresponds to the reduction of the phen moiety of the CPIP ligand.[22] The anodic shift from **1** to **2** is consistent with the higher π deficiency of the TAP moiety of the CPITAP ligand as previously described.[18b] Finally, the reduction waves observed for complexes **3** and **4** correspond to the multiple reduction of the pyridinium unit.[25] From both the cyclic voltammetry measurements and the spectroscopic data, the oxidation and reduction potentials of the excited state can be roughly estimated. From an analysis of these values, complexes **3** and **4** display much higher photo-oxidising power (+1.59 V vs. Ag/AgCl) than complexes **1** and **2**.

Study of the interaction with telomeric G-quadruplex and duplex DNA

A number of biophysical techniques, including optical and fluorescence spectroscopy, melting temperature measurements, CD spectroscopy, isothermal titration calorimetry (ITC) and surface plasmon resonance (SPR), have been developed to study the interactions of ligands with G-quadruplex DNA.[26] In the present study, we performed CD melting temperature measurements (T_m), bio-layer interferometry (BLI) and SPR studies. Due to the very low solubility of complexes **1** and **2** in water, we conducted these studies only on complexes **3** and **4**.

CD spectroscopy and melting assays

First, the ability of complexes **3** and **4** to interact with DNA was investigated by CD experiments with both duplex ($^{5'}CGT_3CGT_5ACGA_3CG^{3'}$ hairpin) and G-quadruplex (wtTel23, $^{5'}TAGGG(TTAGGG)_3{}^{3'}$) DNA. The study was carried out in buffer (10 mM Tris-HCl, pH 7.04) containing 100 mM NaCl or 100 mM KCl. As mentioned in the Introduction, the choice of cation strongly influences the structure of the G-quadruplex. In the sodium buffer, wtTel23 folded into an anti-parallel topology characterised by two positive peaks at 242 and 294 nm, and a negative peak at 262 nm, whereas in the potassium buffer, a maximum was observed at 290 nm with a shoulder at 270 nm, which corresponds to the hybrid-II-type G4. The hairpin duplex DNA was characterised by a negative peak at 251 nm. Upon the addition of complexes **3** and **4** to the sodium-containing buffer, no changes in the CD spectra of wtTel23 and duplex DNA were observed, whereas minor changes in the ellipticity of wtTel23 were observed for complex **3** in potassium buffer. Nevertheless, these results suggest that the complexes did not induce major structural changes into the conformations of G-quadruplex and duplex DNA (see Figures S18–S20 in the Supporting Information). We then performed CD melting assays to assess the thermal stabilisation induced by the interactions of the complexes with wtTel23 and duplex DNA (Figure 2 and Figures S21–S23).

The CD melting curves of wtTel23 and GC-rich hairpin duplex DNA were recorded in the absence or the presence of each complex (at a complex/DNA ratio of 5:1). The results of the CD melting experiments clearly show that complexes **3** and **4** did not significantly alter the stability of the hairpin duplex, whereas a slight stabilisation of wtTel23 with complex **3** was observed in both the sodium and potassium buffers. However, it should be noted that for the studies in the potassium-containing buffer, the measurement was more arduous due to a slight change in the conformation of wtTel23. This was confirmed by observing the CD spectra at different temperatures (see Figure S22 in the Supporting Information). Surprisingly, complex **4** did not stabilise the telomeric sequence in either buffer. This observation has already been described previously with the same ligand CPITAP.[18b] With these results in hand, we continued with more appropriate methods that allowed us to measure kinetic (rate constants for association and dissociation, k_{on} and k_{off}, respectively) and thermodynamic data (dissociation constants, K_D).

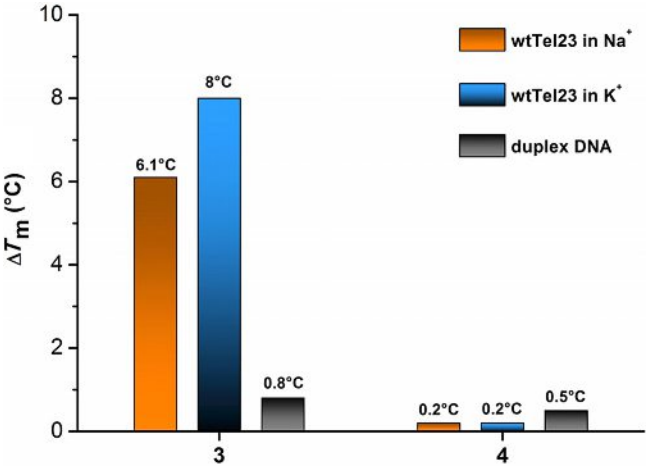

Figure 2. Variation of melting temperatures (ΔT_m) of wtTel23 and duplex hairpin measured between the absence and the presence of complexes **3** and **4**. WtTel23 $^{3'}TT(GGGATT)_3GGG^{5'}$ and hairpin $^{5'}CGT_3CGT_5ACGA_3CG^{3'}$ sequences were first annealed by heating at 95 °C for 5 min in Tris-HCl buffer (10 mM, pH 7.04) with 100 mM NaCl or 100 mM KCl (only for wtTel23) and cooled down overnight to room temperature, then complex **3** or **4** (5 equiv) was added.

Bio-layer interferometry and surface plasmon resonance studies

To determine the thermodynamic and kinetic parameters of the interaction between the complexes and DNA structures, we employed bio-layer interferometry and surface plasmon resonance methods. These methods have previously been used by our group to study the interaction of ruthenium(II) complexes with different G-quadruplex structures.[17b, 18b] In the present study, we performed BLI experiments with both complexes **3** (Figure 3) and **4**. For this investigation, the following systems were used: the intramolecular G-quadruplex **A** (human telomeric sequence (HTelo) with different topologies in equilibrium), the HTelo constrained in a single anti-parallel topology **B** and hairpin DNA **C**. System **B** allows the precise control of the G-quadruplex topology (in this case anti-parallel) through the assembly of constrained structures on a template.[27]

The two complexes **3** and **4** show K_D values in the micromolar range for the G-quadruplex structures **A** and **B** (Table 3 and Figure S24 in the Supporting Information). These values fall within the range of those reported for similar ruthenium(II) complexes interacting with G-quadruplexes. It is noteworthy that the affinity of complex **3** towards G-quadruplex DNA is significantly higher than that of complex **4** (Table 3 and Figure S24). This is in agreement with the melting temperature (T_m) study (see above). However, a weak selectivity for the G-quadruplex structure versus duplex DNA was observed. This could be explained by the net positive charge of the Ir^{III} complexes in comparison with the Ru^{II} complexes that could favour non-specific ionic interactions with the DNA phospho-

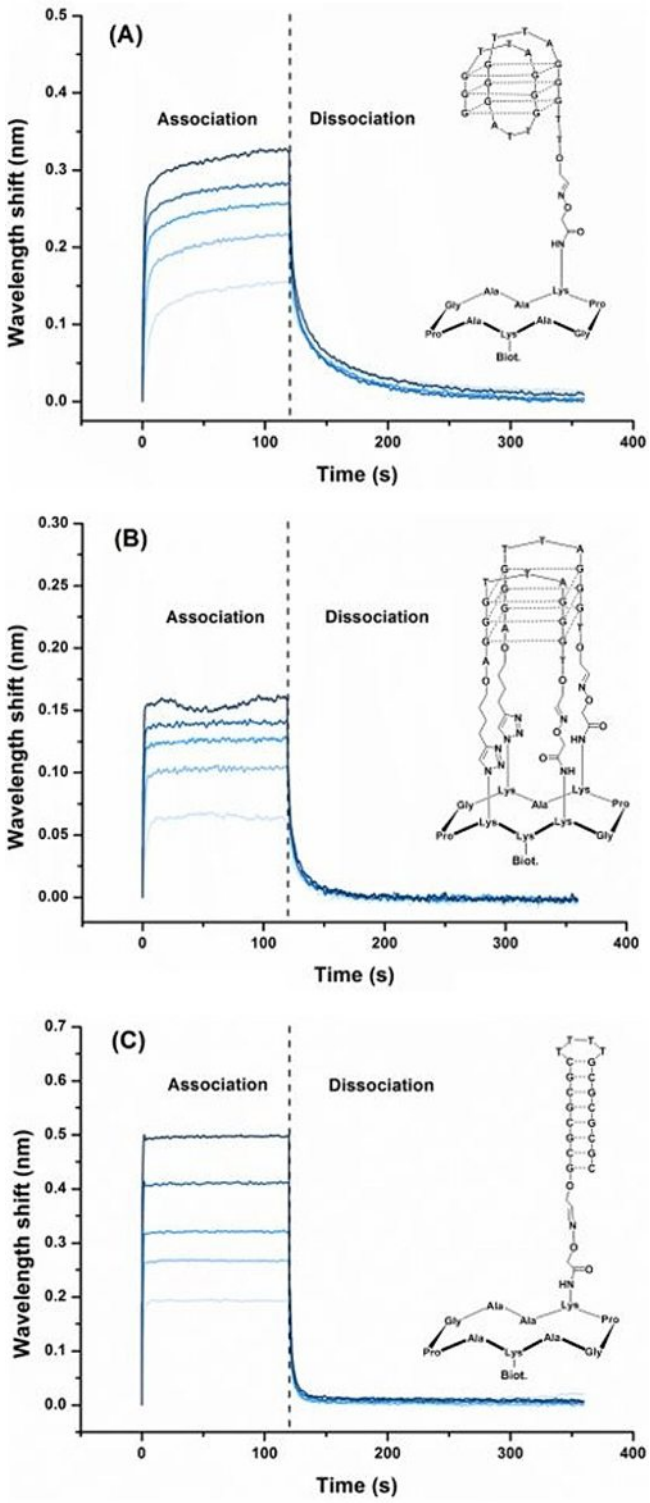

Figure 3. BLI sensorgrams showing the interaction of complex **3** with (A) intramolecular-like G-quadruplex (**A**), (B) human telomeric sequence constrained in an anti-parallel topology (**B**) and (C) hairpin duplex DNA (**C**). The running buffers were 10 mM HEPES (10 mM, pH 7.4) with 35 mM NaCl or 50 mM KCl and 0.5% v/v surfactant.

diester backbone. This is also in agreement with the low ΔT_m value obtained from the CD melting analysis.

To confirm the data obtained from the BLI measurements, SPR analysis was performed with the most promising complex **3** (see Figure S25 and Table S1 in the Supporting Information). For the G-quadruplex structures **A** and **B**, we obtained dissociation constants (K_D) of 4 and 2 μM, respectively. For the duplex hairpin system **C**, a dissociation constant of 28 μM was determined. As anticipated, the values are very close to those obtained from the BLI experiments.

We also compared the kinetic data (k_{on} and k_{off} values, Table 3) determined for complex **3** with those previously reported for similar ruthenium complexes $[Ru(phen)_2(CPIP)]^{2+}$ (**Ru-1**) and $[Ru(TAP)_2(CPIP)]^{2+}$ (**Ru-3**) as well as for well-known G4 ligands (PhenDC3, Braco-19 and TMPyP4).[18b,28] As illustrated in Figure 4, complex **3** shows association and dissociation rate constants similar to those of TMPyP4 and $[Ru(TAP)_2(CPIP)]^{2+}$.

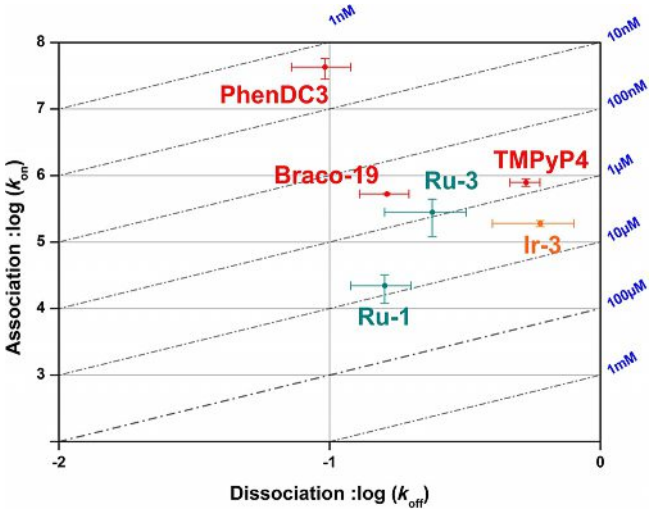

Figure 4. Isoaffinity plot and kinetic characterisation for G-quadruplex structure **B**. For PhenDC3, Braco-19 and TMPyP4 (in red), the analyses were performed by SPR,[28] for the ruthenium(II) complexes (in turquoise)[18b] and iridium(III) complex **3** (in orange) by BLI analysis. k_{on} = association kinetic constant (*y* axis), k_{off} = dissociation kinetic constant (*x* axis) and K_D values are shown by parallel diagonal lines.

Guanine photo-oxidative damage studies

As G-quadruplex DNA are guanine-rich sequences, we investigated the ability of complex **3** to trigger photoinduced electron transfer (PET) with 2′-deoxyguanosine 5′-monophosphate (dGMP). This PET is well known to lead to oxidative lesions in DNA.[29] Based on the electrochemical data, complex **3** has a strong photo-oxidising ability (1.59 V vs. Ag/AgCl) towards guanine (E_{ox} = 1.10 V vs. Ag/AgCl).

Luminescence quenching studies in the presence of dGMP and oligodeoxynucleotides (ODNs)

First, the ability of complex **3** to photo-abstract an electron from a guanine was investigated through luminescence quenching experiments. Figure 5 shows the relative decrease in the emission of complex **3** upon the addition of increasing concentrations of dGMP. A linear Stern–Volmer relationship is obtained from these data (see inset in Figure 5), which sug-

Table 3. Interaction of complexes **3** and **4** with quadruplex DNA **A** and **B**, and duplex DNA **C** structures determined by BLI experiments.

	Quadruplex system **A**			Quadruplex system **B**			Duplex system **C**		
	k_{on} [10^4 M^{-1}s^{-1}]	k_{off} [10^{-1} s^{-1}]	K_D[a] [μM]	k_{on} [10^4 M^{-1}s^{-1}]	k_{off} [10^{-1} s^{-1}]	K_D[a] [μM]	k_{on} [10^4 M^{-1}s^{-1}]	k_{off} [10^{-1} s^{-1}]	K_D[a] [μM]
3	9±2	4±1	4±1	19±2	6±2	3±1	5±1	17±2	34±7
4	3±1	13±1	46±14	3±1	18±2	56±7	1±1	14±1	120±1

[a] Equilibrium dissociation constants deduced from the kinetic rate constants. The errors provided are standard deviations from the mean values. The running buffer was 10 mM HEPES (pH 7.4) with 35 mM NaCl, 50 mM KCl and 0.5% v/v surfactant.

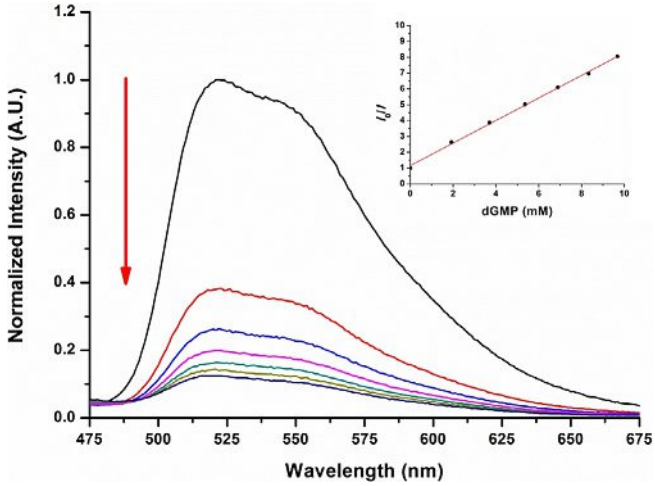

Figure 5. Luminescence titration of complex **3** with dGMP. The experiment was carried out in 50 mM TRIS (pH 7.4) aqueous buffer. The excitation was performed at $\lambda = 350$ nm. Inset: Stern–Volmer plot obtained upon the addition of dGMP (0–10 mM) to **3**.

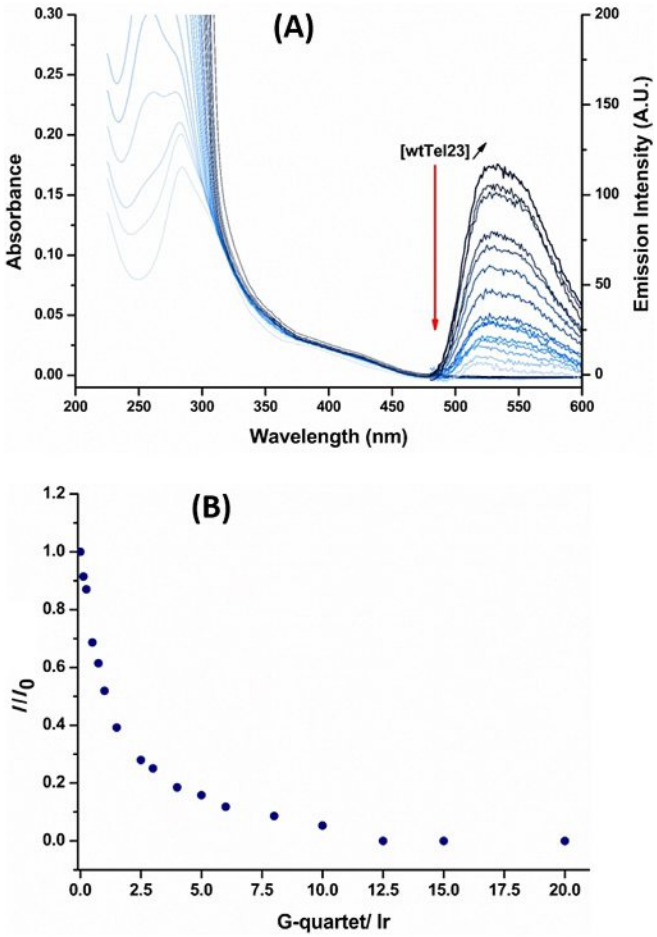

Figure 6. Luminescence titration of complex **3** with the telomeric sequence wtTel23. (A) Absorption and emission spectra upon the addition of increasing concentrations of wtTel23. (B) Luminescence titration of **3** with increasing amounts of G-quadruplex DNA (wtTel23, G-quartet equivalents per Ir complex). Spectra (A, B) were recorded in 10 mM HEPES (pH 7.4), 35 mM NaCl and 50 mM KCl buffer. The excitation was performed at $\lambda = 350$ nm.

gests pure dynamic quenching of the excited state of complex **3** in the presence of dGMP. Considering the oxidation power of the excited state of complex **3** and by using the empirical Rehm–Weller equation, it is expected that process (1) with dGMP will be exergonic by about 0.55 eV. Based on these thermodynamic considerations, we can safely ascribe this luminescence quenching to a photoinduced electron-transfer (PET) process from the guanine unit to the excited state of the complex [reaction (1)].

$$[IrN_4C_2]^{3+*} + G \rightarrow [IrN_4C_2]^{2+} + G^{\bullet+} \quad (1)$$

The efficient quenching in the presence of guanine units is also in agreement with the high value of the quenching rate constant (2.26×10^9 M^{-1}s^{-1}) obtained from the Stern–Volmer plot of complex **3** with dGMP being close to the diffusion limit.

We further tested whether this PET occurs with guanine embedded within an oligonucleotide sequence. We employed the wtTel23 telomeric sequence, which can fold in G-quadruplex DNA in the presence of a buffer solution of 10 mM HEPES, 35 mM NaCl and 50 mM KCl (pH 7.4). Figure 6A displays the absorption and emission spectra recorded upon the addition of increasing concentrations of the telomeric sequence (i.e., wtTel23, $^{5'}$TAGGG(TTAGGG)$_3{}^{3'}$) to complex **3** in the above buffer solution. Only weak changes in the absorption spectrum are observed, as already described for similar metal complexes with DNA.

The luminescence extinction of **3** was monitored by steady-state fluorescence (Figure 6B). The luminescence of **3** was drastically quenched upon the addition of wtTel23. In good agreement with the experiment with dGMP (see above), this luminescence quenching suggests a photoinduced electron transfer (PET) from the guanine-quartet DNA structure. As this elec-

tron transfer (ET) can lead to the formation of oxidised guanine (i.e., 8-oxodG), we further tried to evidence such oxidation products.[29] A control experiment was performed with G-rich duplex DNA (i.e., GC-rich duplex hairpin DNA (HP-GC), $^{3'}$(GC)4TTTT(GC)4$^{5'}$), which showed a lower quenching efficiency (see Figure S26 in the Supporting Information). This suggests a different and better mode of interaction with G-quadruplex DNA.

Photoinduced formation of 8-oxo-dG in the telomeric sequence

It is well known that the oxidation of DNA base pairs can lead to the formation of lesions in the genome.[29] In the present study, we were interested in monitoring the formation of the most common product obtained from oxidation of guanine, that is, 8-oxo-7,8-dihydro-2′-deoxyguanosine (8-oxo-dG). The impact of the formation of 8-oxo-dG on the G-quadruplex structure of the telomeric sequence has been recently studied: depending on the position of 8-oxo-dG in the telomeric sequence, minor or major structural changes can occur.[30] In this context, the development of compounds that can photoinduce the formation of 8-oxo-dG in telomeres is of great interest. Therefore we tested whether the most promising complex **3** is able to increase by PET the prevalence of 8-oxo-dG in the telomeric sequence wtTel23 (Figure 7).

The results of the experiment were compared with those observed with the $[Ru(bpy)_3]^{2+}$ complex, which is well known to induce 8-oxo-dG by type II photo-oxidation (singlet oxygen photosensitisation).[31] The formation of 8-oxo-dG upon irradiation of wtTel23 in the presence of iridium complex **3** was shown and demonstrated the ability of the latter to photoreact with DNA and generate $G^{\bullet+}$. Moreover, the amount of 8-oxo-dG formed upon irradiation in the presence of complex **3** was found to be slightly higher than that observed with $[Ru(bpy)_3]^{2+}$. Nevertheless, a control experiment with G-rich duplex DNA also showed the formation of 8-oxo-dG with similar amount as for the telomeric sequence. These results emphasise the ability of the iridium complex **3** to induce oxidative photolesions in the human genome, even in the structured telomeric sequence.

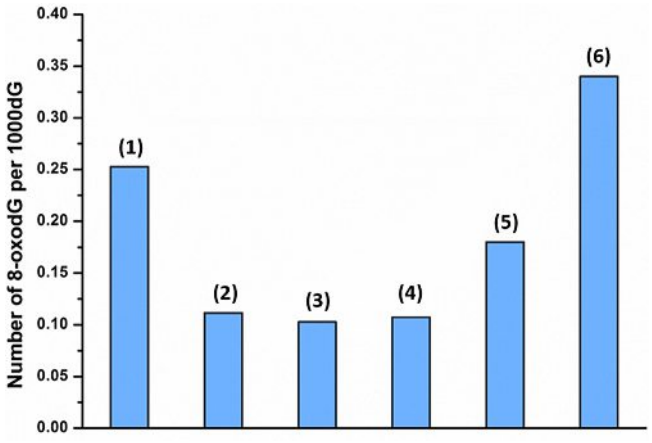

Figure 7. Amount of 8-oxo-dG/1000 dG formed in the telomeric sequence wtTel23 after (1) addition of complex **3** and 30 min irradiation, (2) addition of **3** without irradiation (3) irradiation of wtTel23, (4) wtTel23 in the dark, (5) addition of $[Ru(bpy)_3]^{2+}$ and 30 min irradiation, and (6) control experiment: complex **3** irradiated for 30 min in the presence of the GC-rich duplex hairpin (HP-GC). The photoreactions were performed in a buffer solution of 10 mM HEPES (pH 7.4), 35 mM NaCl and 50 mM KCl.

Conclusions

Three new iridium(III) cyclometallated complexes have been designed and synthesised to target and photoreact with telomeric G-quadruplex DNA. A study of their photophysical properties showed a mixture of transitions for all the complexes. Interestingly, complex **3** displayed good affinity towards telomeric G-quadruplex DNA and a slight selectivity versus duplex DNA. Owing to its oxidising power in the excited state, it is able to photoreact with DNA, likely through a PET from guanine moieties. To the best of our knowledge, this would be the first example of an iridium(III) complex that can interact with G-quadruplex DNA and trigger electron transfer with guanine under light irradiation. This PET leads to the formation of 8-oxo-dG in the telomeric sequence. Nevertheless, no selectivity of this photodamage formation was observed for G-quadruplex versus duplex DNA. This could be due to a too-low a difference of affinity of the iridium complex for G-quadruplex versus duplex DNA. Further efforts have thus to be made to improve the affinity for the G-quadruplex target versus duplex DNA to obtain photoreactive iridium complexes able to selectively target and photodamage the telomeres of cancer cells.

Experimental Section

Material and methods

$[Ir(ppy)_2Cl]_2$,[32] $[Ir(2,2'\text{-}C\text{^}N)_2Cl]_2$,[25] CPIP,[22] CPITAP[18b] and $[Ir(ppy)_2(CPIP)]^+$ (**1**)[22] were synthesised according to previously described literature protocols. All the solvents and reagents for the syntheses were of reagent grade and were used without any further purification. All the solvents for the spectroscopic and electrochemical measurements were of spectroscopic grade. Water was purified with a Millipore Milli-Q system. ^{1}H NMR experiments were performed in CD_3CN on a Bruker AM-500 spectrometer (500 MHz) at 20 °C. The chemical shifts (given in ppm) were measured relative to the residual peak of the solvent as internal standard. HRMS spectra were recorded on a ThermoFisher Q-Extractive orbitrap spectrometer using reserpine as internal standard. The samples were ionised by electrospray ionisation (ESI; capillary temperature = 320 °C, vaporiser temperature = 320 °C, sheath gas flow rate = 5 mL min^{-1}). The studies in acetonitrile and water were performed with the PF_6^- and Cl^- salts, respectively.

Synthesis

$[Ir(ppy)_2(CPITAP)]\cdot PF_6$ (2): $[Ir(ppy)_2Cl]_2$ (20 mg, 0.02 mmol) and CPITAP (13.6 mg, 0.04 mmol) were dissolved in ethylene glycol (2 mL) and heated at 170 °C overnight in the dark and under argon. After cooling and the addition of an aqueous solution of NH_4PF_6, a solid was formed. The latter was washed three times each with water, EtOH and Et_2O to afford the crude product. Purifi-

cation over preparative SiO_2 chromatography ($CH_3CN/H_2O/NH_4Cl$(sat) 4:4:1, v/v/v) and the addition of NH_4PF_6 gave the final product as a red powder (20 mg, 51%). ^{1}H NMR (500 MHz, CD_3CN): $\delta = 9.14$ (s, 2H), 8.26 (m, 4H), 8.07 (d, $J = 8.0$ Hz, 2H), 7.86 (dd, $J = 7.9$ Hz, $J = 0.96$ Hz, 2H), 7.81 (td, $J = 7.6$ Hz, $J = 1.5$ Hz, 2H), 7.63 (d, $J = 11$ Hz, 2H), 7.53 (d, $J = 3.5$ Hz, 2H), 7.12 (td, $J = 7.5$ Hz, $J = 1.2$ Hz, 2H), 7.01 (td, $J = 7.5$ Hz, $J = 1.4$ Hz, 2H), 6.88 (t, $J = 7.2$ H, 2H z), 6.34 ppm (dd, $J = 7.5$ Hz, $J = 0.7$ Hz, 2H); HRMS: calcd for $C_{39}H_{25}N_8ClIr$: 833.151446 [**2**$-PF_6^-]^+$; found: 833.150254.

[Ir(2,2′-C^N)$_2$(CPIP)]·3PF$_6$ (3): [Ir(2,2′-C^N)$_2$Cl]$_2$ (15 mg, 0.009 mmol) and CPIP (6.3 mg, 0.02 mmol) were dissolved in ethylene glycol (2 mL) and heated at 170 °C for 48 h in the dark and under argon. After cooling and the addition of an aqueous solution of NH_4PF_6, a solid was formed. The latter was washed three times each with water, EtOH and Et_2O to afford the crude product. Purification over preparative SiO_2 chromatography ($CH_3CN/H_2O/KNO_3$(sat) 7:0.5:1, v/v/v) and the addition of NH_4PF_6 gave the final product as a yellow powder (12 mg, 53%). ^{1}H NMR (500 MHz, CD_3CN): $\delta = 9.29$ (s, 2H), 8.63–8.59 (d, $J = 8.5$ Hz, 2H), 8.49–8.46 (d, $J = 6$ Hz, 2H), 8.38–8.34 (d, $J = 8.5$ Hz, 2H), 8.24 (m, 2H), 8.12 (t, $J = 8.7$ Hz, 2H), 8.01–7.91 (m, 2H), 7.81–7.73 (m, 2H), 7.67–7.64 (d, $J = 8.5$ Hz, 2H), 7.46–7.41 (dd, $J = 7.7$ Hz, $J = 6.08$ Hz, 2H), 7.34–7.30 (d, $J = 7.7$ Hz, 2H), 7.28 (t, $J = 13.6$ Hz, $J = 6.2$ Hz, 2H), 4.71–4.67 ppm (s, 6H); HRMS: calcd for $C_{41}H_{31}N_8ClF_{12}IrP_2$: 1151.12442 [**3**$-PF_6^-]^{2+}$; found: 1151.12512.

[Ir(2,2′-C^N)$_2$(CPITAP)]·3PF$_6$ (4): [Ir(2,2′-C^N)$_2$Cl]$_2$ (15 mg, 0.009 mmol) and CPITAP (6.3 mg, 0.02 mmol) were dissolved in ethylene glycol (2 mL) and heated at 170 °C for 72 h in the dark and under argon. After cooling and the addition of an aqueous solution of NH_4PF_6, a solid was formed. The latter was washed three times each with water, EtOH and Et_2O to afford the crude product. Purification over preparative SiO_2 chromatography ($CH_3CN/H_2O/KNO_3$(sat) 6:2:2, v/v/v) and the addition of NH_4PF_6 gave the final product as a yellow powder (10 mg, 44%). ^{1}H NMR (500 MHz, CD_3CN): $\delta = 9.29$ (s, 2H), 8.64–8.59 (d, $J = 8.5$ Hz, 2H), 8.52–8.47 (d, $J = 5.3$ Hz, 2H), 8.35 (d, $J = 8.6$ Hz, 2H), 8.31–8.26 (d, $J = 2.6$ Hz, 2H), 8.19–8.13 (t, $J = 9$ Hz, 2H), 7.81 (dd, $J = 5.6$ Hz, $J = 0.9$ Hz, 2H), 7.72–7.65 (d, $J = 8.6$ Hz, 2H), 7.48–7.31 (dd, $J = 7.7$ Hz, $J = 6.1$ Hz, 2H), 7.34–7.28 (t, $J = 5.7$ Hz, 2H), 7.25 (dd, $J = 7.7$ Hz, $J = 0.8$ Hz, 2H), 4.69 ppm (s, 6H); HRMS: calcd for $C_{39}H_{29}N_{10}ClF_{12}IrP_2$: 1153.11492 [**4**$-PF_6^-]^{2+}$; found: 1153.11550.

Absorption and luminescence studies

UV/Vis absorption spectra were recorded on a Shimadzu UV-1700 spectrophotometer. The concentration of the complexes was 10 μM. Room-temperature luminescence spectra were recorded on a Varian Cary Eclipse instrument. Luminescence intensities at 77 K was recorded on a Jobin Yvon FluoroLog3 FL3-22 spectrofluorimeter equipped with an 18 V, 450 W Xenon Short Arc lamp and an R928P photomultiplier along with an Oxford Instrument Optistat DN nitrogen cryostat controlled by an Oxford Intelligent Temperature Controller (ITC503S) instrument. Quantum yields were obtained by using $[Ru(bpy)_3]^{2+}$ as reference.[33] Luminescence lifetime measurements were performed after irradiation at $\lambda = 400$ nm obtained by using the second harmonic of a Titanium:Sapphire laser (picosecond Tsunami laser spectra physics 3950-M1BB + 39868-03 pulse picker doubler) at a repetition rate of 8 MHz or 80 kHz. A Fluotime 200 instrument from AMS technologies was used for the decay acquisition and consists of a GaAs microchannel plate photomultiplier tube (Hamamatsu model R3809U-50) and a time-correlated single photon counting system from Picoquant (PicoHarp300). The ultimate time resolution of the system was close to 30 ps. Luminescence decays were analysed with FLUOFIT software available from Picoquant.

Electrochemical studies

Cyclic voltammetry was carried out in a one-compartment cell using a glassy carbon disk working electrode (approximate area = 0.03 cm^2), a platinum wire counter electrode and an Ag/AgCl reference electrode. The potential of the working electrode was controlled with an Autolab PGSTAT 100 potentiostat through a PC interface. The cyclic voltammograms were recorded with a sweep rate of 100 mV s^{-1} in dried acetonitrile (Sigma-Aldrich, HPLC grade). The concentration of the complexes was 8×10^{-4} mol L^{-1} with 0.1 mol L^{-1} tetrabutylammonium perchlorate as the supporting electrolyte. Before each measurement, the samples were purged with nitrogen. The redox potentials were determined by comparison with ferrocene, added at the end of the measurement.

Luminescence titrations

The dGMP titration experiments with complexes **3** were performed on a Varian Cary Eclipse instrument. A solution of dGMP (5 mM) was progressively added to a solution of complex **3** (50 μM) in 50 mM Tris-HCl buffer (pH 7.4). The luminescence titration spectra of ODN (wtTel23 G-quadruplex DNA and HP-GC duplex DNA) were recorded in 10 mM HEPES, 35 mM NaCl and 50 mM KCl (pH 7.4) buffer on a Varian Cary Eclipse instrument. The titrations were performed with a constant complex concentration (5 μM) and a DNA concentration starting at 10 μM that was progressively decreased.

CD experiments

Prior to the CD analysis, the oligonucleotides were annealed by heating the samples at 95 °C for 5 min in buffer (10 mM Tris buffer, pH 7.04) with 100 mM NaCl or KCl for wtTel23 and 100 mM NaCl for GC-AT hairpin DNA, respectively, followed by cooling overnight to room temperature. The CD analyses were performed on a Jasco J-810 spectropolarimeter using 1 cm length quartz cuvettes. The spectra were recorded every 5 °C, from 25 to 90 °C, in the wavelength range from 220 to 330 nm. For each temperature, the spectrum was an average of three scans with a 0.5 s response time, a 1 nm data pitch, a 4 nm bandwidth and a 200 nm min^{-1} scanning speed. For the CD melting experiments, the ellipticities were recorded at 290 and 252 nm for wtTel23 and the duplex hairpin, respectively. The melting temperatures were measured by Boltzmann fitting to Origin 8.5 software. Each curve fit was only accepted with $r > 0.99$.

Bio-layer interferometry (BLI)

BLI sensors coated with streptavidin (SA sensors) were purchased from Forte Bio (PALL). Prior to use, they were immerged for 10 min in buffer before functionalisation to dissolve the sucrose layer. Then the sensors were dipped for 15 min in DNA-containing solutions (biotinylated systems **A**–**C**) at 100 nM and rinsed in buffer solution (10 mM HEPES (pH 7.4), 35 mM NaCl, 50 mM KCl and 0.5% v/v surfactant P_{20}) for 10 min. The functionalised sensors were next dipped in different iridium(III) complex solutions at different concentrations (see Figure 3 and Figure S24 in the Supporting Information) for 2 min interspersed by a rinsing step in the buffer solution for 4 min. Reference sensors without DNA immobilisation were used to subtract non-specific adsorption on the SA layer. The sensorgrams were fitted by using a heterogeneous model (see Figure 3 and Figure S24). The reported values are the means of

representative independent experiments, and the errors provided are standard deviations from the mean. Each experiment was repeated at least twice.

Quantification of 8-oxo-dG by LC-MS-MS

The samples containing 100 μM of complex with 10 nmol of ODN (wtTel23 or HP-GC) in 200 μL of 10 mM HEPES (pH 7.4), 35 mM NaCl and 50 mM KCl buffer were irradiated (or not) during 30 min with a blue LED system. 8-Oxo-dG was quantified by HPLC coupled through electrospray ionisation to tandem mass spectrometry (HPLC-MS/MS) as detailed previously[34] subsequent to enzymatic digestion of the oligonucleotides.

Acknowledgements

This work was supported by the Fonds de la Recherche Scientifique-FNRS (Grant no. J.0091.18). J.W. thanks the "Fonds pour la Formation à la Recherche dans l'Industrie et dans l'Agriculture" (F.R.I.A.) and the Erasmus programme for financial support. This work was partially supported by the "Agence National de la Recherche" (ANR-16-CE11-0006-01), Labex ARCANE and CBH-EUR-GS (ANR-17-EURE-0003) and the région Auvergne-Rhône-Alpes. The NanoBio-ICMG platforms (FR 2607) are acknowledged for their support. We also thank Dr. L. Bonnat and Dr. T. Lavergne for providing biomolecular systems **A**–**C**.

Conflict of interest

The authors declare no conflict of interest.

Keywords: DNA structures · iridium · ligand design · photoinduced electron transfer · photophysics

[1] S. Neidle, S. Balasubramanian, *Quadruplex Nucleic Acids*, RSC Biomolecular Sciences, Cambridge, **2006**.
[2] V. S. Chambers, G. Marsico, J. M. Boutell, M. Di Antonio, G. P. Smith, S. Balasubramanian, *Nat. Biotechnol.* **2015**, *33*, 877.
[3] A. Bedrat, L. Lacroix, J.-L. Mergny, *Nucleic Acids Res.* **2016**, *44*, 1746.
[4] D. Rhodes, H. J. Lipps, *Nucleic Acids Res.* **2015**, *43*, 8627 – 8637.
[5] M. Métifiot, S. Amrane, S. Litvak, M.-L. Andreola, *Nucleic Acids Res.* **2014**, *42*, 12352 – 12366.
[6] K. Paeschke, T. Simonsson, J. Postberg, D. Rhodes, H. J. Lipps, *Nat. Struct. Mol. Biol.* **2005**, *12*, 847 – 854.
[7] R. J. O'Sullivan, J. Karlseder, *Nat. Rev. Mol. Cell Biol.* **2010**, *11*, 171 – 181.
[8] N. Grandin, M. Charbonneau, *Biochimie* **2008**, *90*, 41 – 59.
[9] S. Victorelli, J. F. Passos, *EBioMedicine* **2017**, *21*, 14 – 20.
[10] D. Hanahan, R. A. Weinberg, *Cell* **2011**, *144*, 646 – 674.
[11] A. J. Cesare, R. R. Reddel, *Nat. Rev. Genet.* **2010**, *11*, 319 – 330.
[12] a) H. Han, L. H. Hurley, *Trends Pharmacol. Sci.* **2000**, *21*, 136 – 142; b) D. Monchaud, M.-P. Teulade-Fichou, *Org. Biomol. Chem.* **2008**, *6*, 627 – 636; c) I. M. Dixon, F. Lopez, A. M. Tejera, J.-P. Estève, M. A. Blasco, G. Pratviel, B. Meunier, *J. Am. Chem. Soc.* **2007**, *129*, 1502 – 1503; d) E. M. Rezler, J. Seenisamy, S. Bashyam, M.-Y. Kim, E. White, W. D. Wilson, L. H. Hurley, *J. Am. Chem. Soc.* **2005**, *127*, 9439 – 9447.
[13] a) Q. Cao, Y. Li, E. Freisinger, P. Z. Qin, R. K. O. Sigel, Z.-W. Mao, *Inorg. Chem. Front.* **2017**, *4*, 10 – 32; b) S. N. Georgiades, N. H. Abd Karim, K. Suntharalingam, R. Vilar, *Angew. Chem. Int. Ed.* **2010**, *49*, 4020 – 4034; *Angew. Chem.* **2010**, *122*, 4114 – 4128.
[14] S. Neidle, *Nat. Rev. Chem.* **2017**, *1*, 0041.
[15] a) T.-C. Liao, T.-Z. Ma, Z. Liang, X.-T. Zhang, C.-Y. Luo, L. Liu, C.-Q. Zhou, *Chem. Eur. J.* **2018**, *24*, 15840 – 15851; b) C. Q. Zhou, T. C. Liao, Z. Q. Li, J. Gonzalez-Garcia, M. Reynolds, M. Zou, R. Vilar, *Chem. Eur. J.* **2017**, *23*, 4713 – 4722; c) A. Ali, M. Kamra, S. Roy, K. Muniyappa, S. Bhattacharya, *Bioconjugate Chem.* **2017**, *28*, 341 – 352.
[16] a) R. Kieltyka, P. Englebienne, J. Fakhoury, C. Autexier, N. Moitessier, H. F. Sleiman, *J. Am. Chem. Soc.* **2008**, *130*, 10040 – 10041; b) K. J. Castor, Z. Liu, J. Fakhoury, M. A. Hancock, A. Mittermaier, N. Moitessier, H. F. Sleiman, *Chem. Eur. J.* **2013**, *19*, 17836 – 17845.
[17] a) E. Wachter, D. Moyá, S. Parkin, E. C. Glazer, *Chem. Eur. J.* **2016**, *22*, 550 – 559; b) G. Piraux, L. Bar, M. Abraham, T. Lavergne, H. Jamet, J. Dejeu, L. Marcélis, E. Defrancq, B. Elias, *Chem. Eur. J.* **2017**, *23*, 11872 – 11880; c) L. Xu, X. Chen, J. Wu, J. Wang, L. Ji, H. Chao, *Chem. Eur. J.* **2015**, *21*, 4008 – 4020; d) X. Wang, L. Pei, X. Fan, S. Shi, *Inorg. Chem. Commun.* **2016**, *72*, 7 – 12.
[18] a) S. A. Archer, A. Raza, F. Dröge, C. Robertson, A. J. Auty, D. Chekulaev, J. A. Weinstein, T. Keane, A. J. H. M. Meijer, J. W. Haycock, S. MacNeil, J. A. Thomas, *Chem. Sci.* **2019**, *10*, 3502 – 3513; b) J. Weynand, M. Abraham, A. Diman, L. Marcélis, H. Jamet, A. Decottignies, J. Dejeu, E. Defrancq, B. Elias, *Chem. Eur. J.* **2018**, *24*, 19216 – 1922.
[19] D. Xia, B. Wang, B. Chen, S. Wang, B. Zhang, J. Ding, L. Wang, X. Jing, F. Wang, *Angew. Chem. Int. Ed.* **2014**, *53*, 1048 – 1052; *Angew. Chem.* **2014**, *126*, 1066 – 1070.
[20] a) C. Lentz, O. Schott, T. Auvray, G. Hanan, B. Elias, *Inorg. Chem.* **2017**, *56*, 10875 – 10881; b) A. Jacques, O. Schott, K. Robeyns, G. Hanan, B. Elias, *Eur. J. Inorg. Chem.* **2016**, 1779 – 1783.
[21] a) L. Lu, W. Wang, C. Yang, T.-S. Kang, C.-H. Leung, D.-L. Ma, *J. Mater. Chem. B* **2016**, *4*, 6791 – 6796; b) S. Lin, W. Wang, C. Hu, G. Yang, C.-N. Ko, K. Ren, C-H. Leung, D.-L. Ma, *J. Mater. Chem. B* **2017**, *5*, 479 – 484; c) S. Lin, L. Lu, T.-S. Kang, J.-L. Mergny, C.-H. Leung, D.-L. Ma, *Anal. Chem.* **2016**, *88*, 10290 – 10295; d) L. Lu, M. Wang, Z. Mao, T.-S. Kang, X.-P. Chen, J.-J. Lu, C.-H. Leung, D.-L. Ma, *Sci. Rep.* **2016**, *6*, 22458.
[22] K. J. Castor, K. L. Metera, U. M. Tefashe, C. J. Serpell, J. Mauzeroll, H. F. Sleiman, *Inorg. Chem.* **2015**, *54*, 6958 – 6967.
[23] a) A. Jacques, A. Kirsch-De Mesmaeker, B. Elias, *Inorg. Chem.* **2015**, *54*, 6958 – 6967; b) R. Bevernaegie, L. Marcélis, B. Laramée-Milette, J. De Winter, K. Robeyns, P. Gerbaux, G. S. Hanan, B. Elias, *Inorg. Chem.* **2018**, *57*, 1356 – 1367.
[24] K. Laws, A. Eskandari, C. Lu, K. Suntharalingam, *Chem. Eur. J.* **2018**, *24*, 15205 – 15210.
[25] a) B. J. Coe, M. Helliwell, S. Sanchez, M. K. Peers, N. S. Scrutton, *Dalton Trans.* **2015**, *44*, 15420 – 15423; b) B. J. Coe, M. Helliwell, J. Raftery, S. Sanchez, M. K. Peers, N. S. Scrutton, *Dalton Trans.* **2015**, *44*, 20392 – 20405.
[26] P. Murat, Y. Singh, E. Defrancq, *Chem. Soc. Rev.* **2011**, *40*, 5293 – 5307.
[27] a) P. Murat, D. Cressend, N. Spinelli, A. Van der Heyden, P. Labbé, P. Dumy, E. Defrancq, *ChemBioChem* **2008**, *9*, 2588 – 2591; b) P. Murat, R. Bonnet, A. Van der Heyden, N. Spinelli, P. Labbé, D. Monchaud, M.-P. Teulade-Fichou, P. Dumy, E. Defrancq, *Chem. Eur. J.* **2010**, *16*, 6106 – 6114; c) R. Bonnet, T. Lavergne, B. Gennaro, N. Spinelli, E. Defrancq, *Chem. Commun.* **2015**, *51*, 4850 – 4853.
[28] L. Bonnat, J. Dejeu, H. Bonnet, B. Génnaro, O. Jarjayes, F. Thomas, T. Lavergne, E. Defrancq, *Chem. Eur. J.* **2016**, *22*, 3139 – 3147.
[29] a) D. B. Hall, R. E. Holmlin, J. K. Barton, *Nature* **1996**, *382*, 731 – 735; b) C. J. Burrows, J. G. Muller, *Chem. Rev.* **1998**, *98*, 1109 – 1151; c) J.-L. Ravanat, C. Saint-Pierre, J. Cadet, *J. Am. Chem. Soc.* **2003**, *125*, 2030 – 2031; d) T. Lindahl, *Nature* **1993**, *362*, 709 – 715.
[30] S. Bielskute, J. Plavec, P. Podbevšek, *J. Am. Chem. Soc.* **2019**, *141*, 2594 – 2603.
[31] G. Sathyaraj, M. Kiruthika, T. Weyhermüller, B. Unni Nair, *Dalton Trans.* **2012**, *41*, 8460 – 8471.
[32] S. Sprouse, K. A. King, P. J. Spellane, R. J. Watts, *J. Am. Chem. Soc.* **1984**, *106*, 6647 – 6653.
[33] A. M. Brouwer, *Pure Appl. Chem.* **2011**, *83*, 2213 – 2228.
[34] J.-L. Ravanat, T. Douki, P. Duez, E. Gremaud, K. Herbert, T. Hofer, L. Lasserre, C. Saint-Pierre, A. Favier, J. Cadet, *Carcinogenesis* **2002**, *23*, 1911 – 1918.

Manuscript received: May 13, 2019
Revised manuscript received: July 2, 2019
Accepted manuscript online: July 10, 2019
Version of record online: August 29, 2019